Microstructures in shocked quartz: linking nuclear airbursts and meteorite impacts

TEXT, METHODS

SAMPLES

METEOR CRATER. This sample was collected in 1966 by co-author T.E.B on the rim ~500 m north of the center of the crater at ~35.032206° N, 111.023988° W.

JOE-1/4. This sample was obtained in 2011 at the Semipalatinsk test site by Dr. Byron Ristvet, DTRA, with permission from the Kazakhstan National Nuclear Center and the Russian Federation Atomic Energy Agency. The gross sample was sifted to obtain the fine sand studied here.

TRINITY. A sediment sample "JIE" was obtained in 2003 at the Trinity Site near ground zero by Jim Eckles of the White Sands Missile Range Public Affairs Office. The gross sample was sifted to remove fines as well as larger rocks, resulting in the thin section of sand that was used for this study. Sample "meltglass" was obtained in 2011 at the Trinity Site about 400 meters NNE from ground zero, where it landed after being ejected from the detonation. It was collected by co-author R.E.H. with permission from the White Sands Missile Range Public Affairs office, a slice of which was thin-sectioned for this study.

PROCESSING STEPS

(i) Sediment was wet-sieved to concentrate grains between diameters of ~150 (#100 ASTM sieve) to ~850 μm (#20 ASTM sieve).

(ii) Typically, the sorted grains were treated with HCl to destroy carbonates.

(iii) Grains were embedded in blue epoxy for better visibility, covering the entire 27 x 46 mm slide, and were sectioned at Spectrum Petrographics, Vancouver, WA. Sectioned slides were given a high-polish, microprobe-grade finish, necessary for EBSD analyses. No cover slide was used.

(iv) Slides were etched with HF vapor at 50% concentration for ~2 min. Note that exposure for <2 min was insufficient for etching and exposing shock fractures; exposure for >2 min can damage the slides.

(v) Grains were examined using a petrographic polarizing microscope with a rotary stage. The microscope was equipped with transmitted light and epi-illumination (reflected light). First, epi-illumination was used and then, transmitted light with objectives ranging from 04x to 100x magnification. Once a candidate grain was identified, it was rotated to extinction under cross polars. Photomicrographs were acquired under both transmitted light and epi-illumination.

(vi) After re-polishing the etched grains to a microprobe finish using 50 nm colloidal silica, SEM imagery was acquired.

(vii) Next, the elemental compositions of individual grains were determined using SEM-based EDS.
(viii) Cathodoluminescence was recorded in both panchromatic (185–850 nm wavelengths) and 3-filtered (RGB) formats. Because red, green, and blue channels were optimized individually to obtain the maximum amount of information from the image, color information in the images is non-quantitative.
(ix) EBSD analyses were performed using multiple routines.
(x) FIB foils were extracted from selected quartz grains.
(xi) TEM analyses were performed on individual foils.
(xii) Elemental compositions of the grains were determined using TEM-based EDS. FFTs and bi-plots of d-spacing and intensity were produced with Digital Micrograph, version 3.32.2403.0. Because electron microscopy is capable of causing irradiation-induced amorphization[1], quartz grains were examined at low magnification using low voltages and short image-acquisition times.

ANALYTICAL DETAILS

HF ETCHING. Following Bunch et al.[2], Spectrum Petrographics, Vancouver, WA etched thin-sectioned slides by exposure to HF vapor for 2 min to dissolve amorphous quartz and make any lamellae more visible. After treatment with HF vapor, we performed another dH_2O rinse.

Alternately, we treated some slides with liquid HF for 2 min, after which we performed a dH_2O rinse; neutralized them with 5% sodium carbonate solution; rinsed them with dH_2O again; then treated them with 5% HCl to remove carbonates. The vapor produced more consistent results. Multiple studies[3-8] have demonstrated the utility of etching quartz grains with HF to differentiate between glass-filled shock features and glass-free tectonic deformation lamellae. In our study, we observed that HF will also sometimes lightly etch tectonic deformation lamellae to reveal broad, shallow depressions, as has been reported by others[5,7]. However, unlike shock fractures, these depressions in the damaged lattice do not extend more than a few microns into the grain and were not observed to contain amorphous silica.

SEM AND SEM-EDS. At Elizabeth City State University, North Carolina, analyses were conducted in low-vacuum mode using a JEOL-6000 SEM system. At the University of Oregon, we used a ThermoFisher Apreo 2 SEM with a CL detector. Using SEM-EDS, we manually selected for detection of major elements with uncertainties of approximately ±10%. At the University of Utah, secondary and backscattered electron images were collected using a Teneo SEM system (Thermofisher FEI, Hillsboro, OR).

TEM, STEM, and TEM-EDS. At the CAMCOR facility at the University of Oregon, Transmission/Scanning transmission electron microscopy, or (S)TEM, was performed on an FEI 80-300 Titan scanning/transmission electron microscope (STEM), equipped with an image corrector, High-Angle Annular Dark Field (HAADF) detector, Energy Dispersive X-ray Spectroscopy (EDS) detector, Gatan Imaging Filter (GIF), and a 4-megapixel Charge-Coupled Device (CCD) camera. Microscope magnification was calibrated using a standard cross-grating

carbon replica (2,160 lines/mm) evaporated with Au-Pd (Ted Pella #607). All images, diffraction patterns, and EDX maps were collected at 300Kv and processed using Digital Micrograph, version 3.32.2403.0.

At the University of Utah, STEM/TEM was performed on a JEOL 2800 operated at 200 kV. EDS data was collected and processed using ThermoFisher Noran System 7 software. Spectral maps were processed as net-counts (background subtracted), using a 5x5 kernel size. Quantitative results were obtained using the Cliff-Lorimer method, with absorption correction.

FOCUSED ION BEAM. At the CAMCOR facility of the University of Oregon, TEM samples of quartz foils were prepared using a Helios Dual Beam SEM FIB. At the Surface Analysis Laboratory at the University of Utah, TEM sample preparation of quartz foils from bulk specimens was performed on an FEI/Thermo Helios Nanolab 650. The lift-out procedure followed standard sample preparation techniques. An electron beam deposited platinum layer as first locally deposited. Next, an ion-beam platinum layer was deposited. Trenches were milled on each side of the protective layer. Cuts were then made to the underside and a micromanipulator probe was placed in contact with the surface (Omniprobe 200). The probe was attached by depositing platinum and then the sample was cut free from the bulk. Using the micromanipulator probe, the lift-out was attached to a copper support grid. The sample was then thinned using the ion beam at progressively decreasing accelerating voltages, 30kV, 16kV, 8kV, and 2kV.

CATHODOLUMINESCENCE. At the University of Oregon, cathodoluminescent (CL) images were synchronously captured at red (R), green (G), and blue (B) wavelengths on coated thin sections in low-vacuum mode on a Thermo Apreo2 S FE-SEM at 10kV using 3.2nA of beam current at ~10 mm working distance with 50Pa of chamber pressure to balance charge. Individual images using red, blue, and green wavelength filters on the CL detector were acquired and composited to create a 24-bit color image. Wavelength ranges: red: 595-813 nm; green: 495-615; and blue: 291-509 nm. Backscatter (BSE), and secondary (SE) electron images were captured with similar beam settings.

EBSD. At the University of Utah, secondary and backscattered electron SEM images were collected using a Teneo system (Thermofisher FEI; Hillsboro, OR). EDS, EBSD, and CL analyses were similarly conducted with the same SEM system installed with the following detectors. An Octane Elite EDS system (EDAX, Pleasanton, CA) was used to collect elemental spectra. A Monarc CL Detector (Gatan; Pleasanton, CA) was used for cathodoluminescence studies. SEM beam energy and current were optimized to meet the requirements of each analysis mode. Before imaging, sample slides were polished to 0.20 μm roughness with colloidal silica suspension and then washed with water to remove residues. The slides were then coated with 5-nm-thick carbon using a Leica EM ACE600 coater (Leica Microsystems, Inc., Deerfield, IL) to prevent charging during the imaging process.

MICRO-RAMAN. We investigated the shock fractures using micro-Raman with poor results. Even after highly polishing the quartz grains, their extensive fractures and amorphization inhibited the acquisition of usable Raman spectra.

UNIVERSAL STAGE. We also investigated the shock fractures using the universal stage. However, we could not determine Miller indices because the observed shock fractures are non-planar and thus, cannot be accurately measured and compared to planar features.

FIGURES

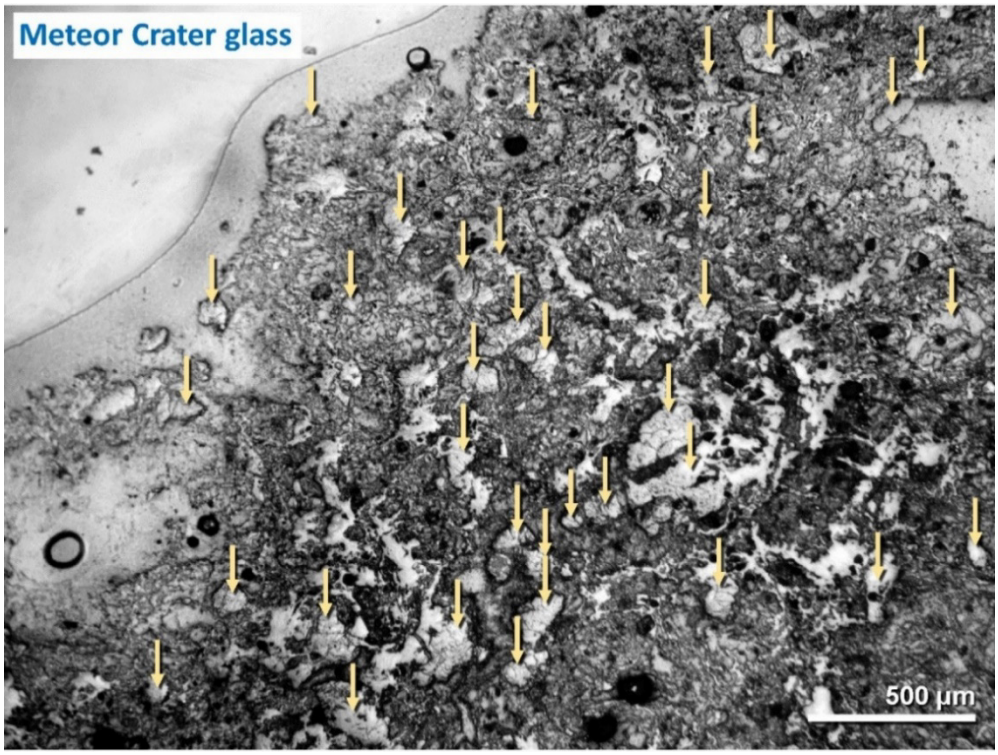

Figure S1. Meltglass containing shock-fractured quartz from Meteor Crater. Epi-photomicrograph of a thin-sectioned slide. We analyzed ~36 quartz grains (arrows) displaying shock fractures in a fragment of ejected meltglass. Shock-fractured grains were concentrated at ~600 quartz grains per cm^2**.**

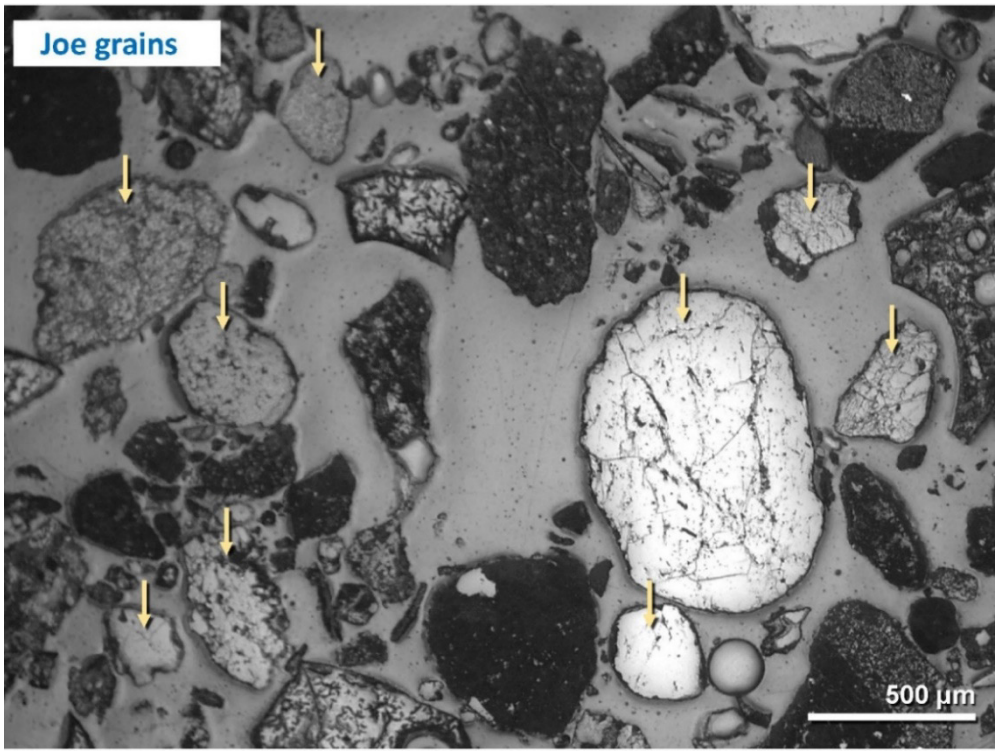

Figure S2. Shock-fractured quartz grains from the Joe-1/4 atomic test site. Epi-photomicrograph of a thin-sectioned slide. We analyzed ~24 loose grains (9 shown at arrows) with shock fractures. Extracted from test site sediment at a concentration of ~150 quartz grains per cm^2.

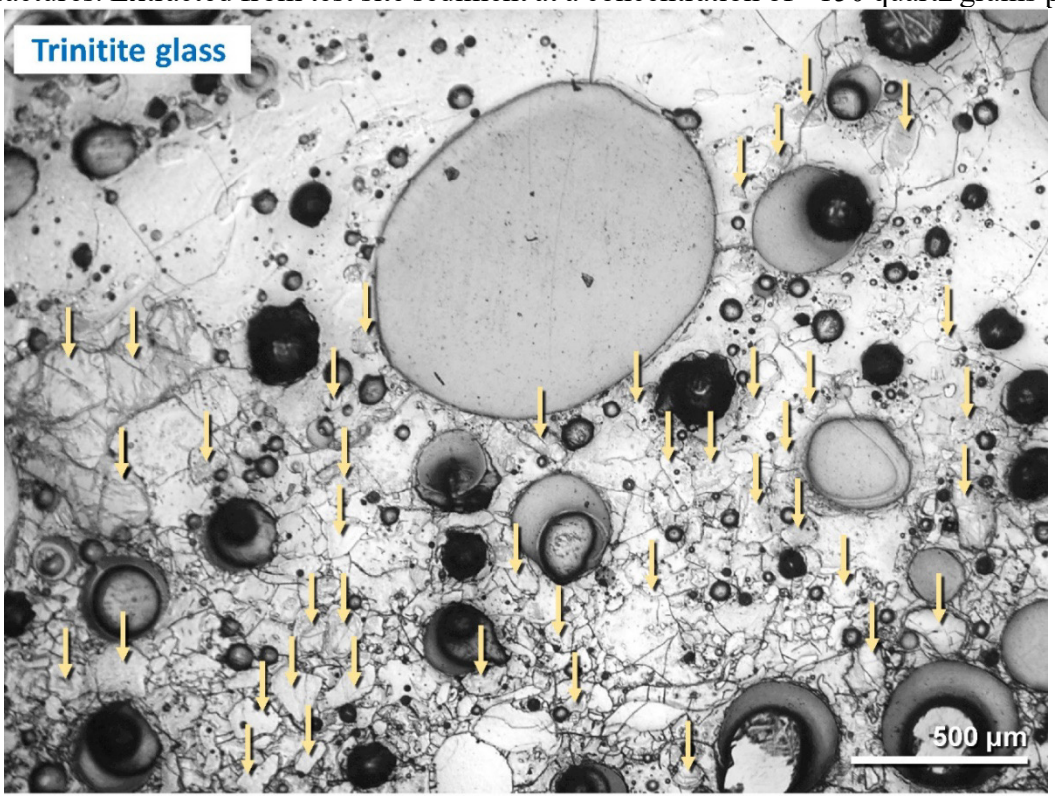

Figure S3. Shock-fractured quartz grains in Trinity meltglass. Epi-photomicrograph of a thin-sectioned slide. We analyzed 42 grains (arrows) with shock fractures from ejected meltglass at a concentration of ~700 quartz grains per cm^2.

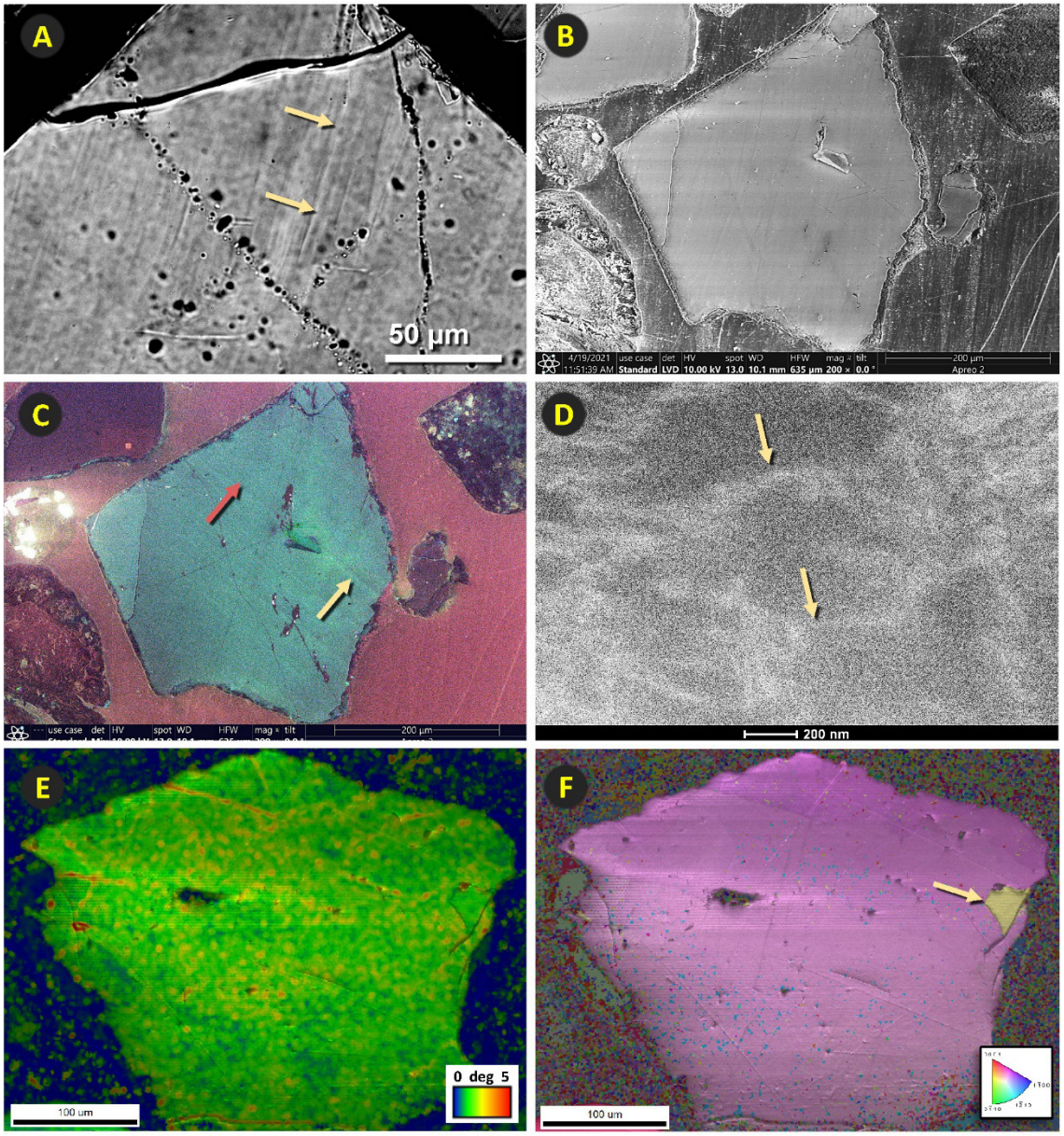

Figure S4. Tectonically-deformed quartz from northern Syria. (A) Optical microscopy image shows tectonically-deformed lamellae. **(B)** SEM image: tectonic lamellae are not visible on the surface. **(C)** Cathodoluminescence (CL); the tectonic lamellae are faintly visible as blue streaks in the grain. Blue luminescence indicates the quartz is normal and unshocked[8-11]. The red arrow marks the extraction location of the ion beam (FIB) foil for use with TEM. **(D)** TEM; there are no parallel lamellae, only lighter areas at the arrows characteristic of dislocations in the quartz. **(E)** EBSD image quality (IQ) and local orientation spread (LOS): there are no significantly aligned misorientations. **(F)** EBSD IQ and inverse pole figure (IPF); the single Dauphiné twin (arrow) is not oriented with any features in the grain, except the single fracture to the right of it. Thus, in this grain, the tectonic lamellae are only visible in the optical and CL images and not in other analyses, as they are in shock fractures. These multiple techniques allow differentiation between non-shock tectonic lamellae and fractures formed by impact-related shock.

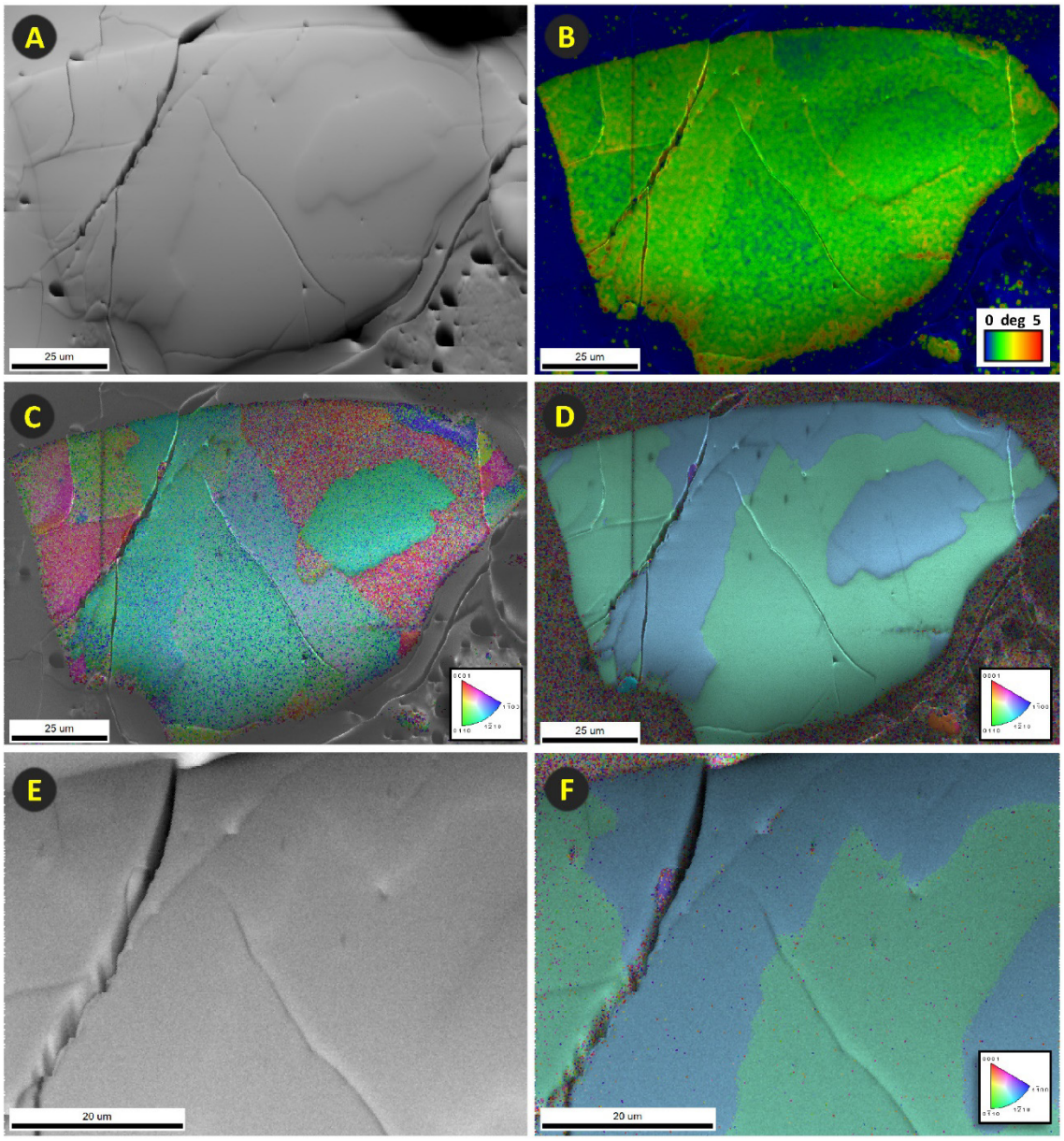

Figure S5. Natural, fractured, and unshocked quartz from the Russian Joe-1/4 site. **(A)** EBSD SEM-like virtual backscatter image shows a few fractures but they are not filled with glass. **(B)** EBSD image quality superimposed on local orientation spread shows no shock fractures aligned with locally misoriented lattice. **(C)** EBSD image quality (IQ) and grain reference orientation deviation (GROD) show no pattern of misoriented lattice compared to the grain's average orientation. **(D)** EBSD image quality (IQ) and inverse pole figures (IPF) illustrate variations in the lattice axes of quartz relative to a chosen crystal reference frame, which for these grains is the (0001) basal plane. There are Dauphiné twins (blue) but they are not globally oriented with the fractures. **(E**) Close-up SEM image of quartz grain. **(F)** SEM and EBSD inverse pole figures. This grain is fractured but the fractures are not oriented as in shock fractures. In addition, no amorphous silica was found associated with the lamellae. No well-oriented lamellae are visible in any of these images.

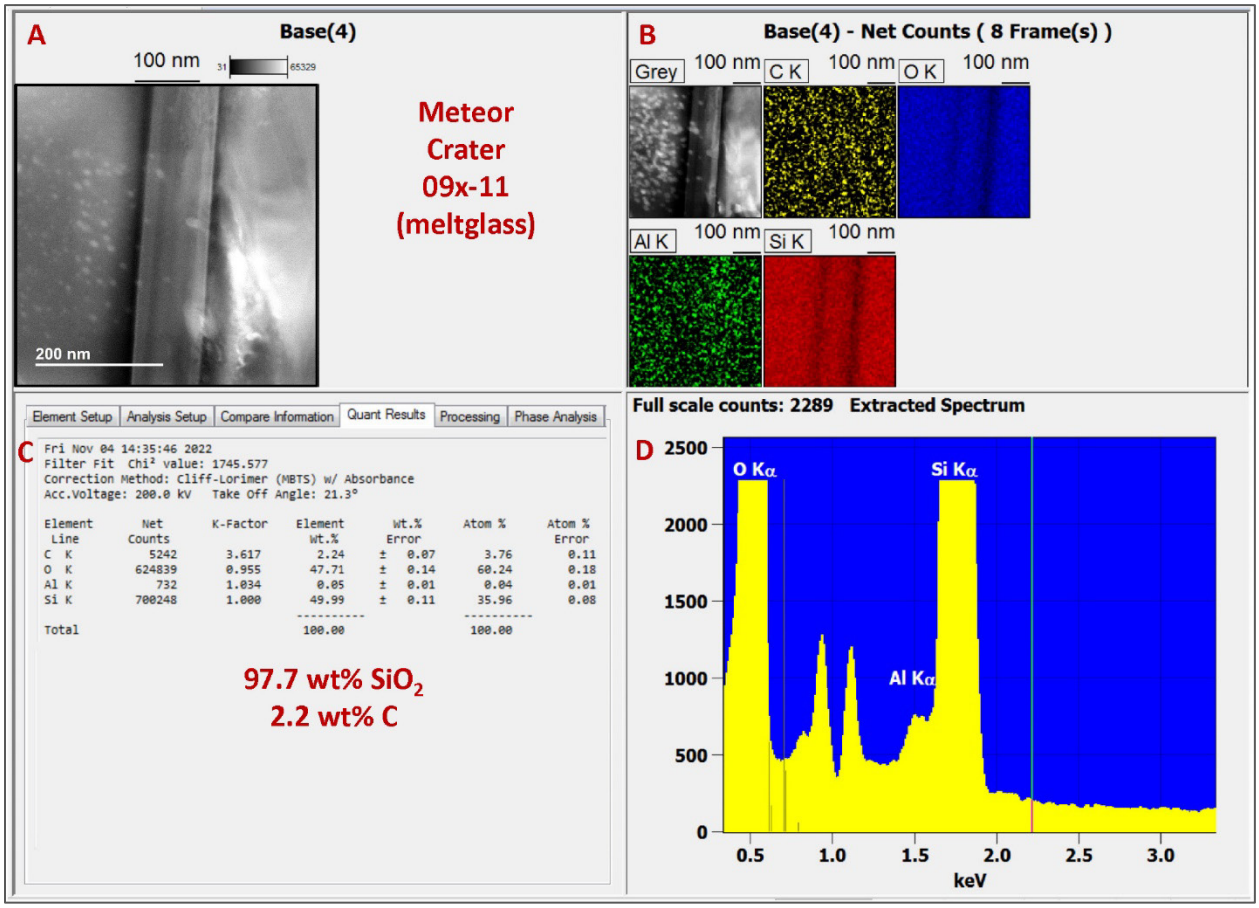

Figure S6. TEM-EDS data for Meteor Crater grain 09x-11. 97.7 wt% SiO_2, 2.2 wt% C, and 0.05 wt% Al. Note that the C and Al are distributed evenly across the foil, suggesting that they are contamination from processing the sample. **(A)** TEM image showing area with amorphous silica (center) in the grain. EDS analyses were made on the entire field of view. **(B)** Panels showing concentrations of selected elements. **(C)** Elemental concentrations were measured for the entire field of view. **(D)** Energy spectrum for various elements of EDS analysis. These descriptions also apply to captions for **Figs. S7-S9** below.

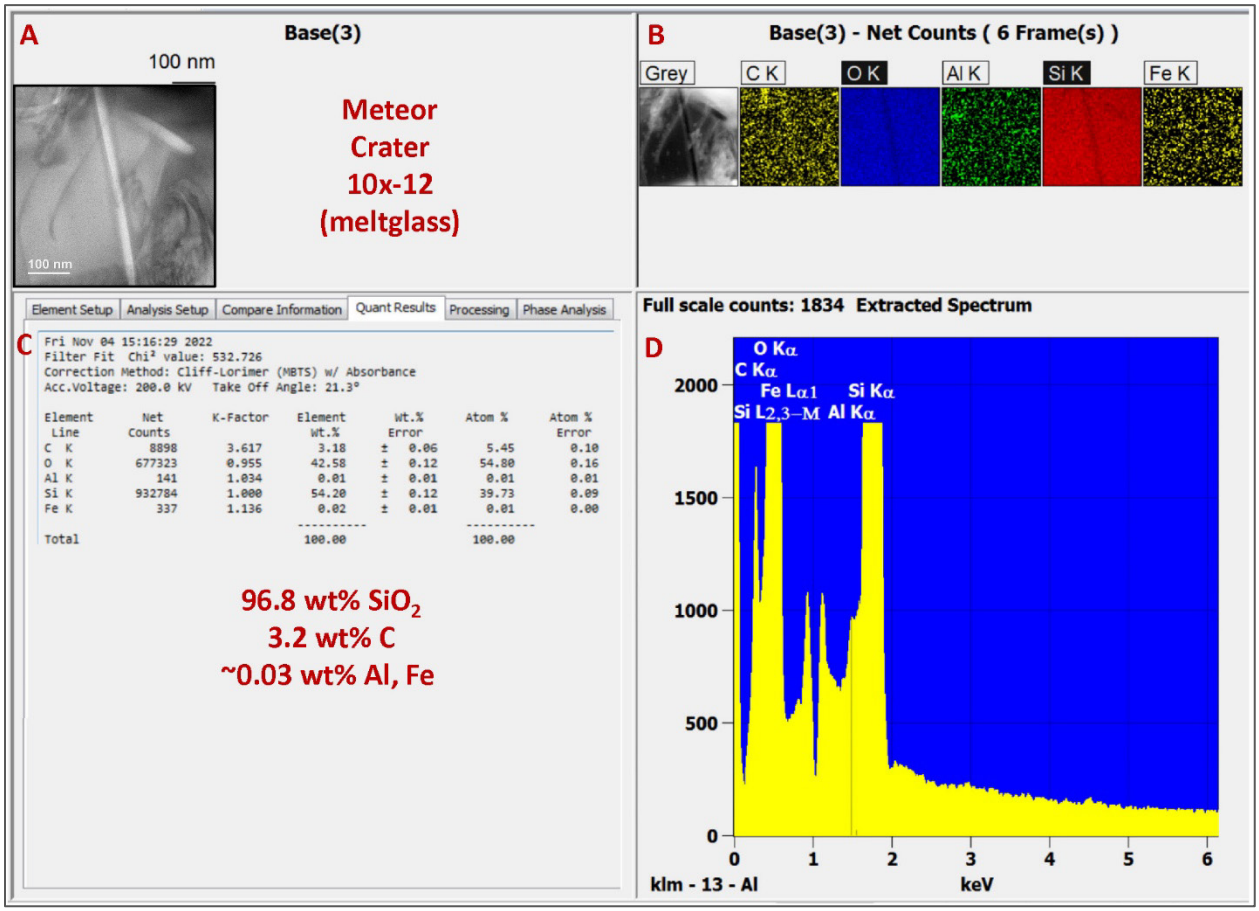

Figure S7. TEM-EDS data for Meteor Crater grain 10x-12. 96.8 wt% SiO_2, 3.2 wt% C, 0.02 wt% Fe, and 0.01 wt% Al. Note that the C, Fe, and Al appear to be contaminants introduced during the processing of the sample. For descriptions of panels, see the caption for **Fig. S6**.

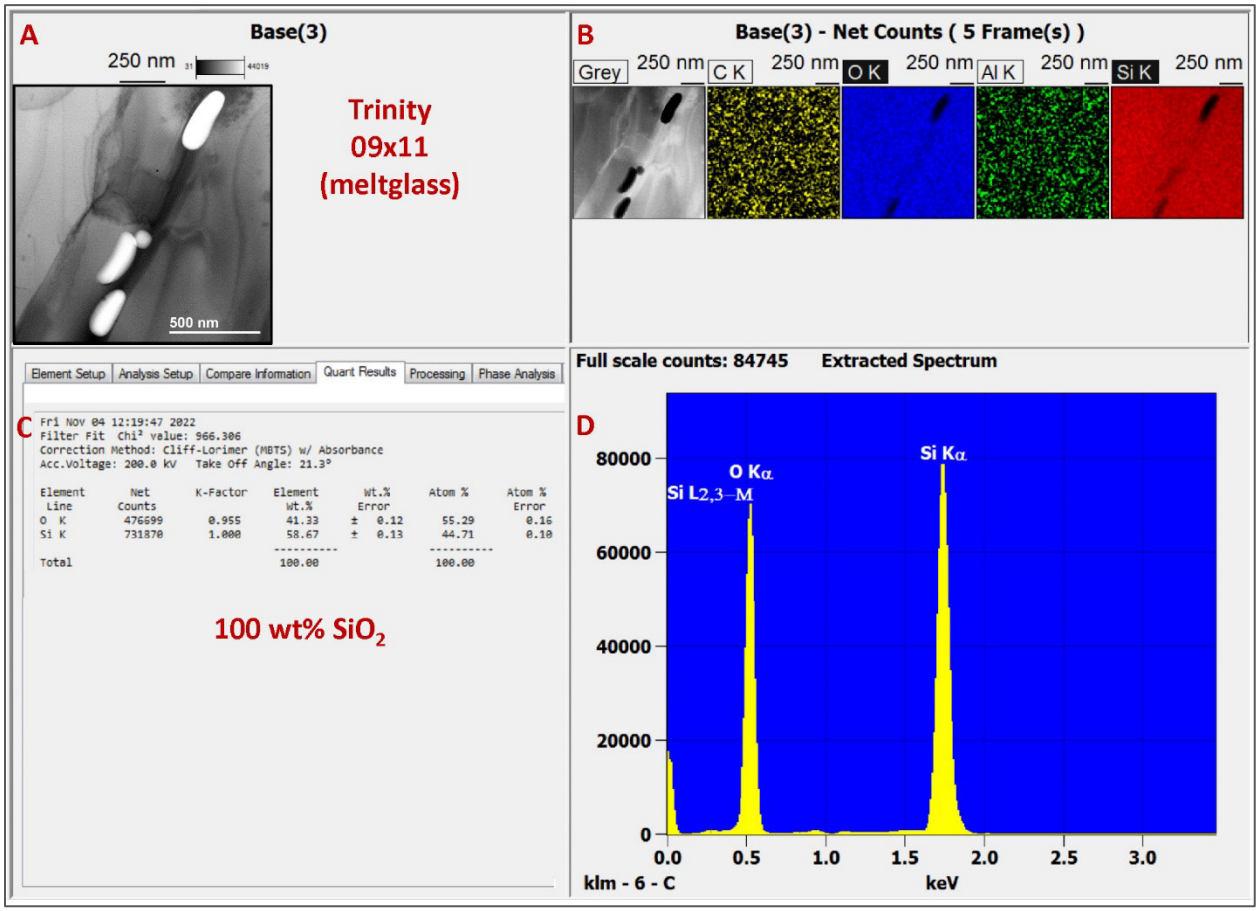

Figure S8. TEM-EDS data for Trinity meltglass grain 09x11. ~100 wt% SiO_2 with negligible amounts of Al and C, most likely contamination from processing the sample. For descriptions of panels, see the caption for **Fig. S6**.

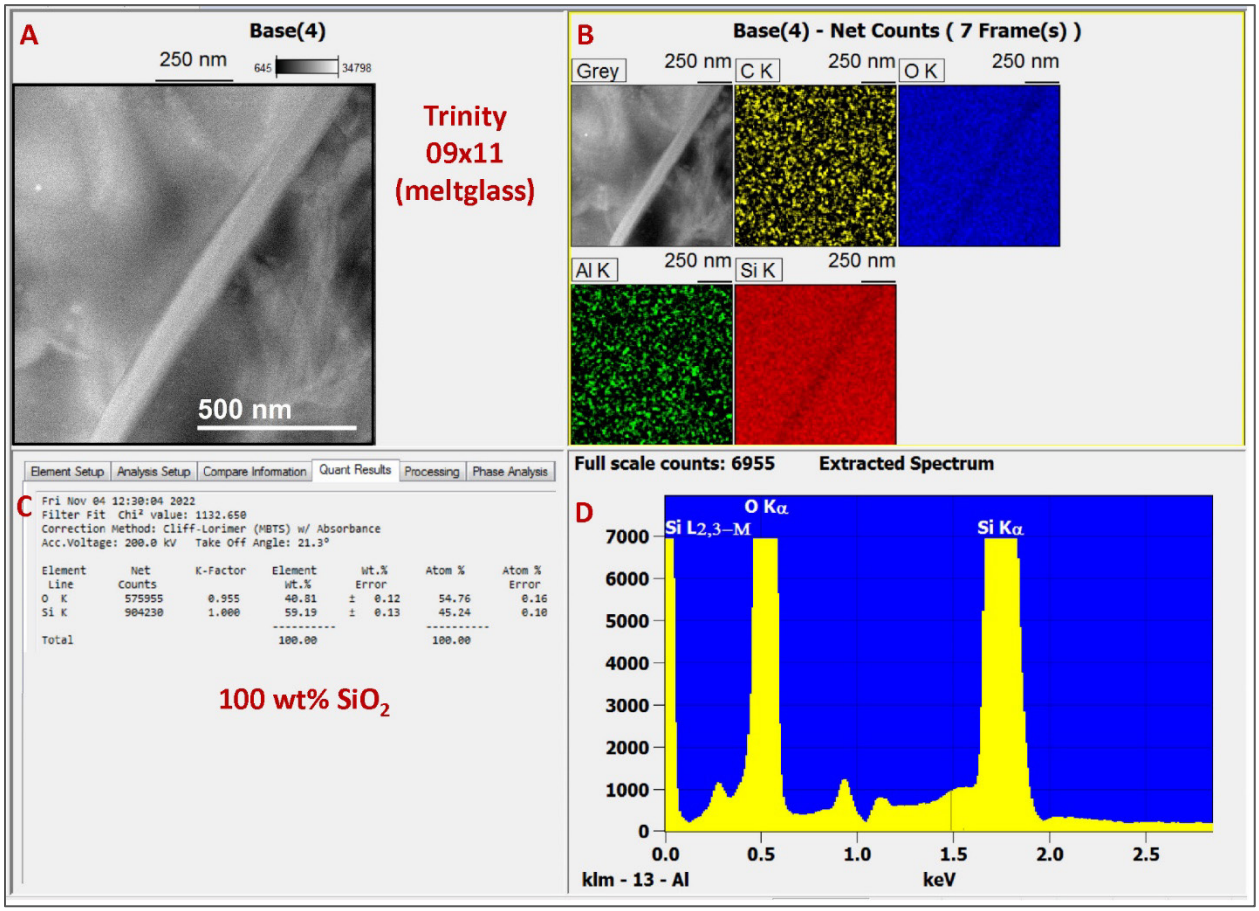

Figure S9. Additional TEM-EDS data for Trinity meltglass grain 09x11. ~100 wt% SiO_2 with insignificant amounts of Al and C, most likely contamination from processing the sample. For descriptions of panels, see the caption for **Fig. S6**.

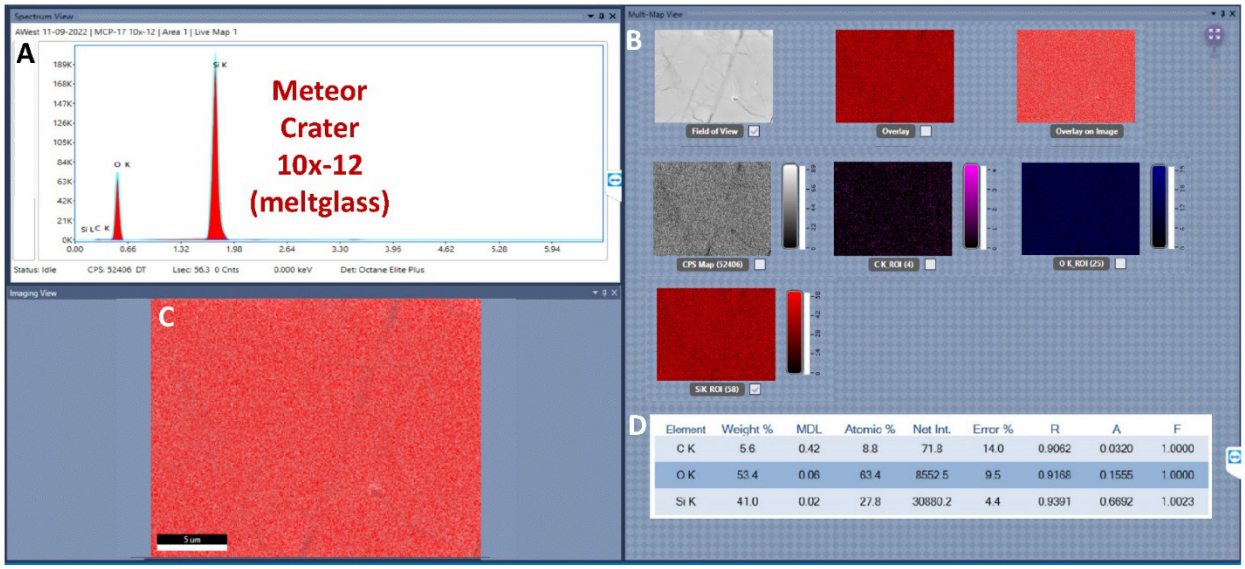

Figure S10. SEM-based EDS spectrum for Meteor crater grain 10x-12. (A) Energy spectrum for various elements of EDS analysis. EDS analyses were made on the entire field of view. **(B)** Panels showing concentrations of selected elements. **(C)** Composite image showing silicon panel

overlying the SEM field of view. **(D)** Elemental concentrations were measured for the entire field of view. These descriptions also apply to captions for **Figs. S11-S14** below.

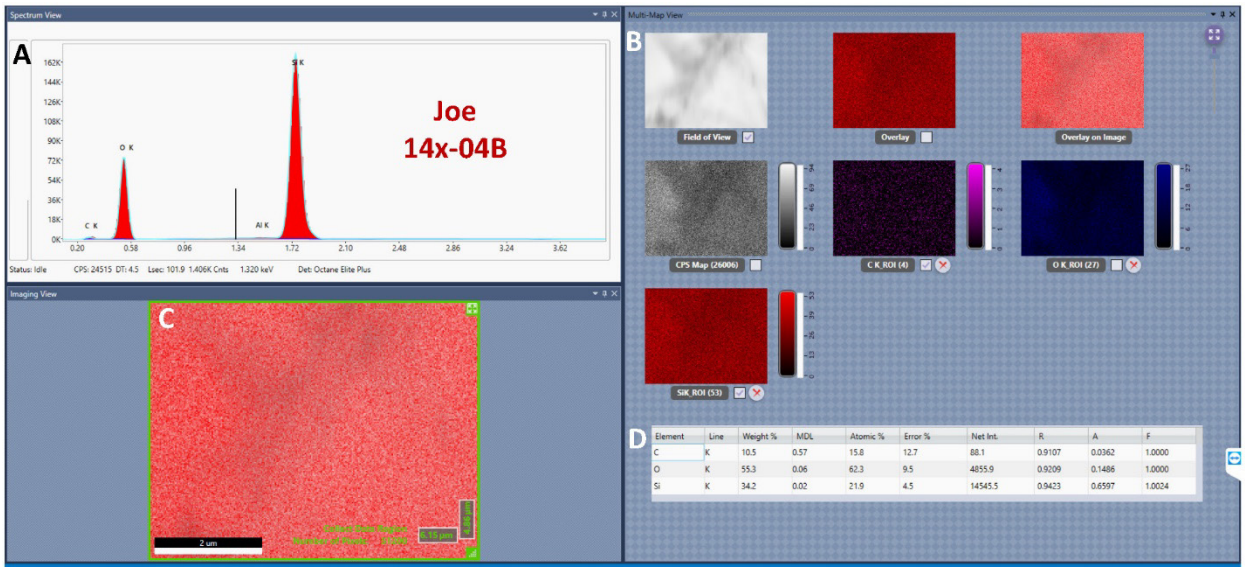

Figure S11. SEM-based EDS spectrum for Joe-1/4 grain 14x-04B. For descriptions of panels **(A)-(D)**, see the caption for **Fig. S10**.

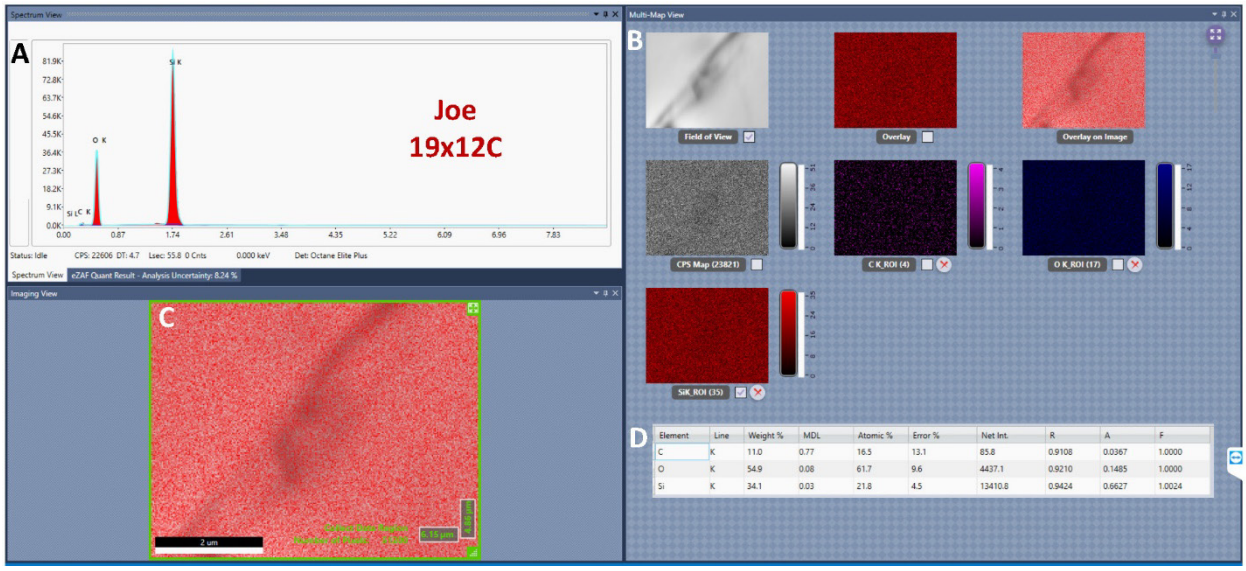

Figure S12. SEM-based EDS spectrum for Joe-1/4 grain 19x-12C. For descriptions of panels **(A)-(D)**, see the caption for **Fig. S10**.

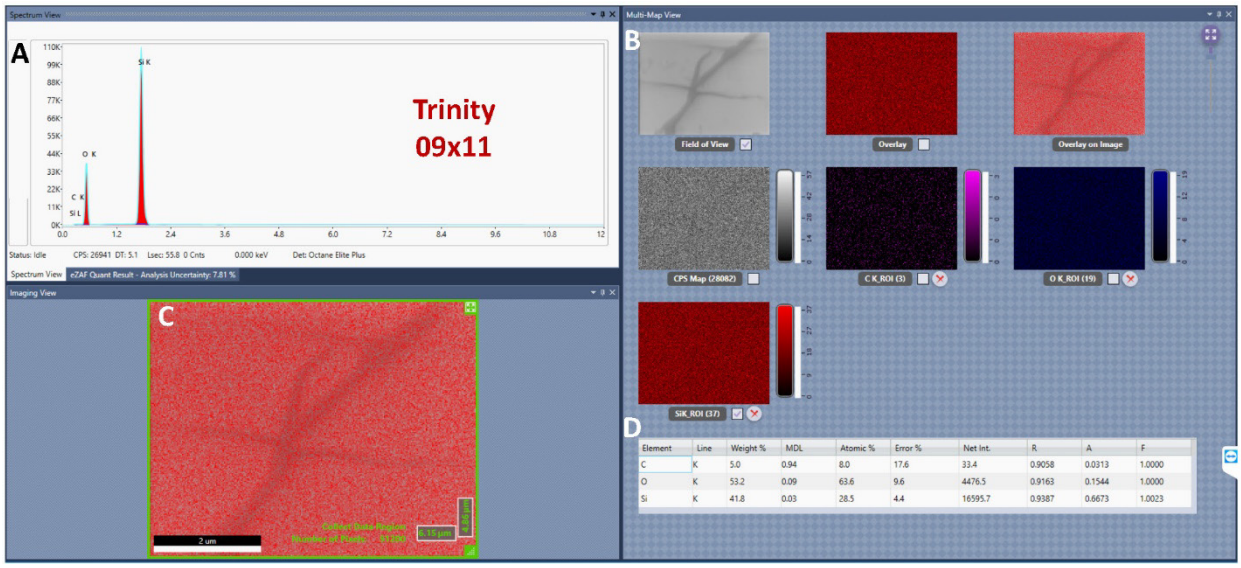

Figure S13. SEM-based EDS spectrum for Trinity meltglass grain 09x11. For descriptions of panels **(A)-(D)**, see the caption for **Fig. S10**.

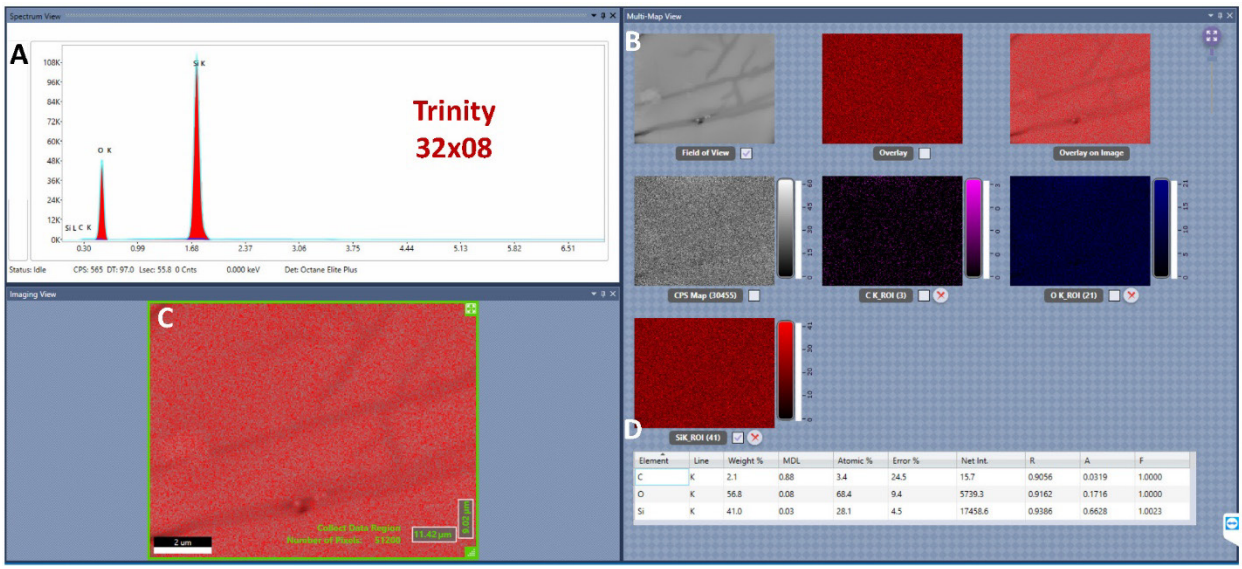

Figure S14. SEM-based EDS spectrum for Trinity meltglass grain 32x08. For descriptions of panels **(A)-(D)**, see the caption for **Fig. S10**.

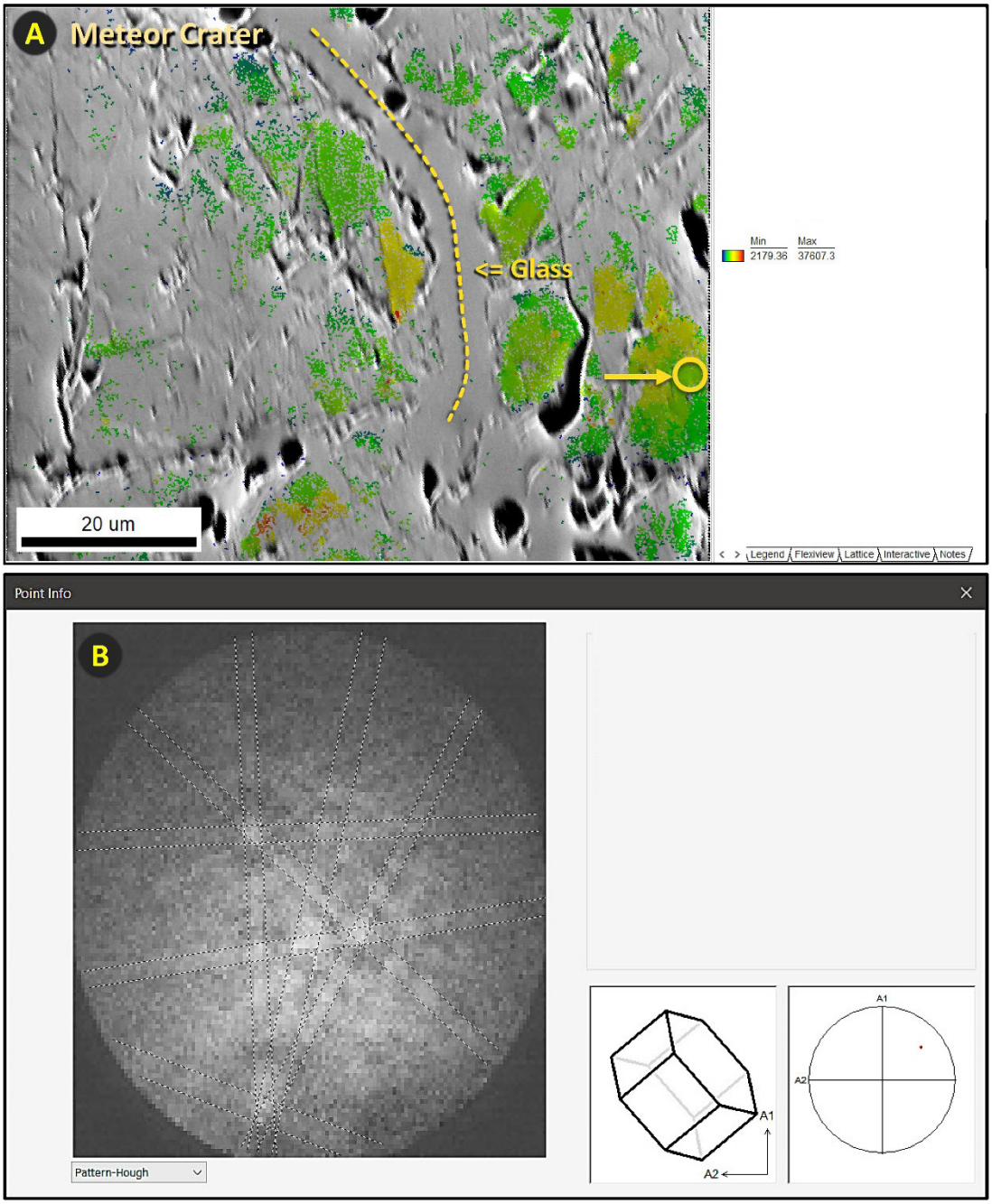

Figure S15. EBSD Kikuchi patterns of shock-fractured quartz. (A) Meteor Crater grain 10x-12. EBSD image of virtual backscatter results (similar to SEM-BSE image) overlain by the grain average image quality. Blue/green/yellow/red colors denote decreasing image quality. Gray color represents areas where no Kikuchi patterns were detected, suggesting the area is amorphous or has short-range ordering of crystals. The gray area along the dashed yellow line is interpreted as a region of amorphous silica that intruded into the grain or melted *in situ*. **(B)** For EBSD analyses, the diffracted electrons produce what are called Kikuchi patterns that reveal the microstructural properties of the sample. The panel shows an EBSD Kikuchi pattern from a spot in the yellow circle in panel A. The lattice diagram at the lower right represents the grain's crystalline structure in which the hexagonal surface is the basal plane, (0001), with the c-axis perpendicular to it.

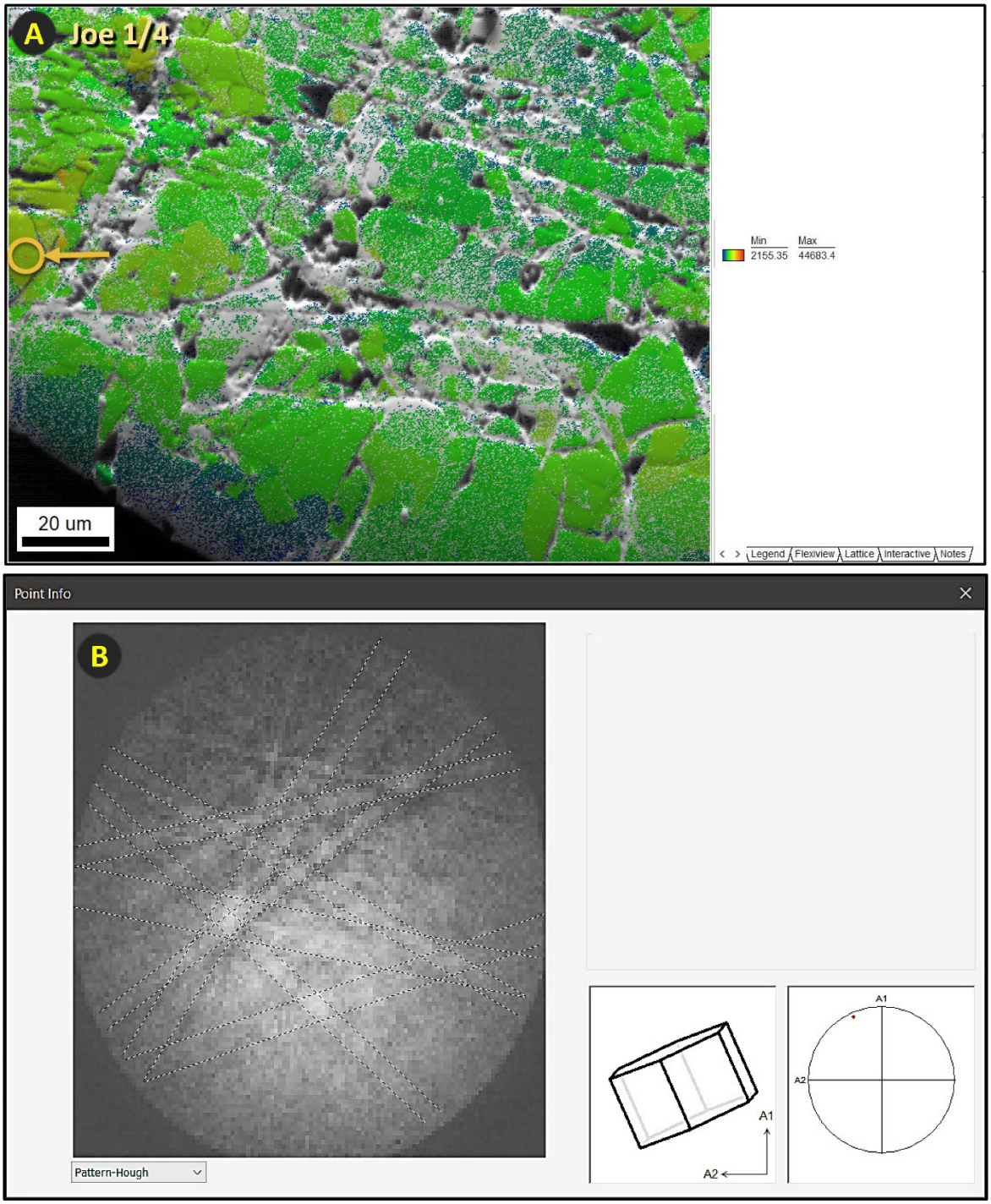

Figure S16. EBSD Kikuchi patterns of shock-fractured quartz. (A) Joe-1/4 grain 14x-04B. EBSD image of virtual backscatter results (similar to SEM-BSE image) overlain by the grain average image quality. Blue/green/yellow/red colors denote decreasing image quality. Gray color represents areas where no Kikuchi patterns were detected, suggesting the area is amorphous or has short-range ordering of crystals. **(B)** EBSD Kikuchi pattern from a spot in the yellow circle in panel A. The lattice diagram at the lower right represents the grain's crystalline structure in which the hexagonal surface is the basal plane, (0001), with the c-axis perpendicular to it.

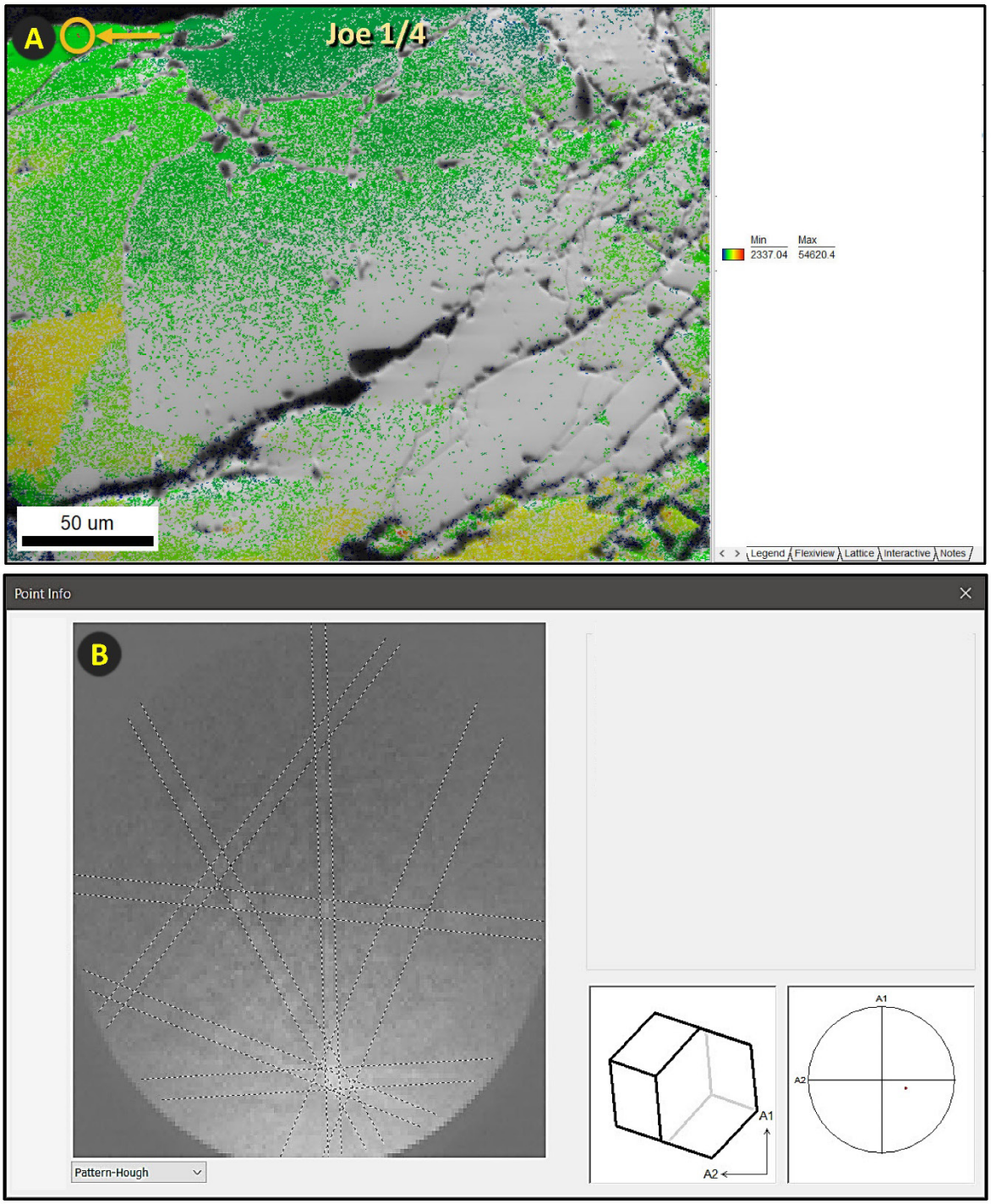

Figure S17. EBSD Kikuchi patterns of shock-fractured quartz. **(A)** Joe-1/4 grain 19x-12C. EBSD image of virtual backscatter results (similar to SEM-BSE image) overlain by the grain average image quality. Blue/green/yellow/red colors denote decreasing image quality. Gray color represents areas where no Kikuchi patterns were detected, suggesting the area is amorphous or has short-range ordering of crystals. **(B)** EBSD Kikuchi pattern from a spot in the yellow circle in panel A. The lattice diagram at the lower right represents the grain's crystalline structure in which the hexagonal surface is the basal plane, (0001), with the c-axis perpendicular to it.

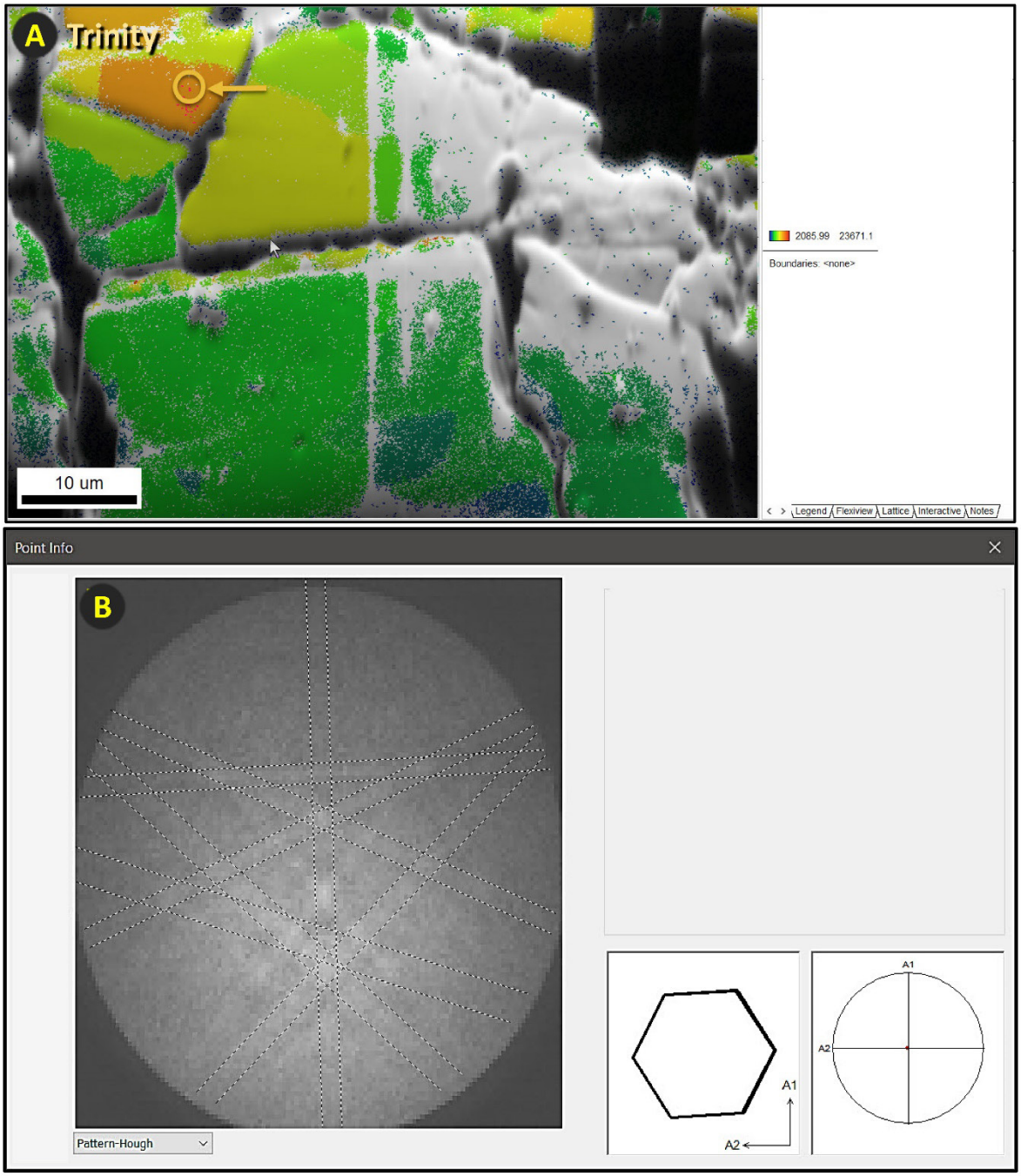

Figure S18. EBSD Kikuchi patterns of shock-fractured quartz. **(A)** Trinity meltglass grain 32x08. EBSD image of virtual backscatter results (similar to SEM-BSE image) overlain by the grain average image quality. Blue/green/yellow/red colors denote decreasing image quality. Gray color represents areas where no Kikuchi patterns were detected, suggesting the area is amorphous or has short-range ordering of crystals. **(B)** EBSD Kikuchi pattern from a spot in the yellow circle in panel A. The lattice diagram at the lower right represents the grain's crystalline structure in which the hexagonal surface is the basal plane, (0001), with the c-axis perpendicular to it.

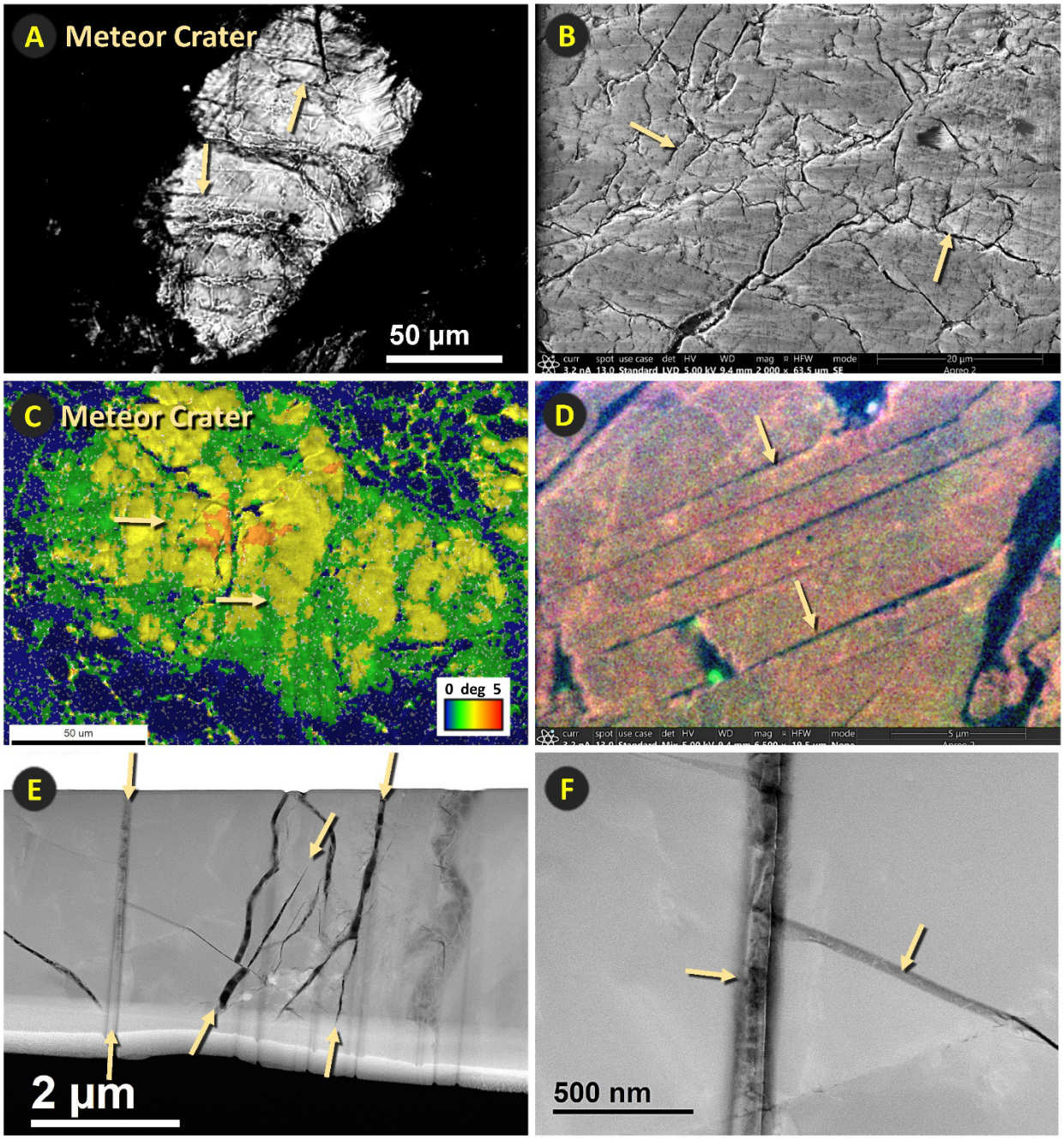

Figure S19. Images of selected portions of shock-fractured quartz grain 09x-11 from Meteor Crater. A) Optical photomicrograph. Selected shock fractures are marked by arrows. **(B)** SEM image. **(C)** EBSD image quality (IQ) and grain average image quality (GAIQ). Green areas at the arrows represent areas that correspond with shock fractures. (**D**) Cathodoluminescence (CL) image of non-luminescent gray-to-black areas at arrows indicating amorphous silica in areas corresponding to oriented shock fractures. **(E)** TEM image of open, glass-filled shock fractures. **(F)** Close-up TEM image of glass-filled shock fractures.

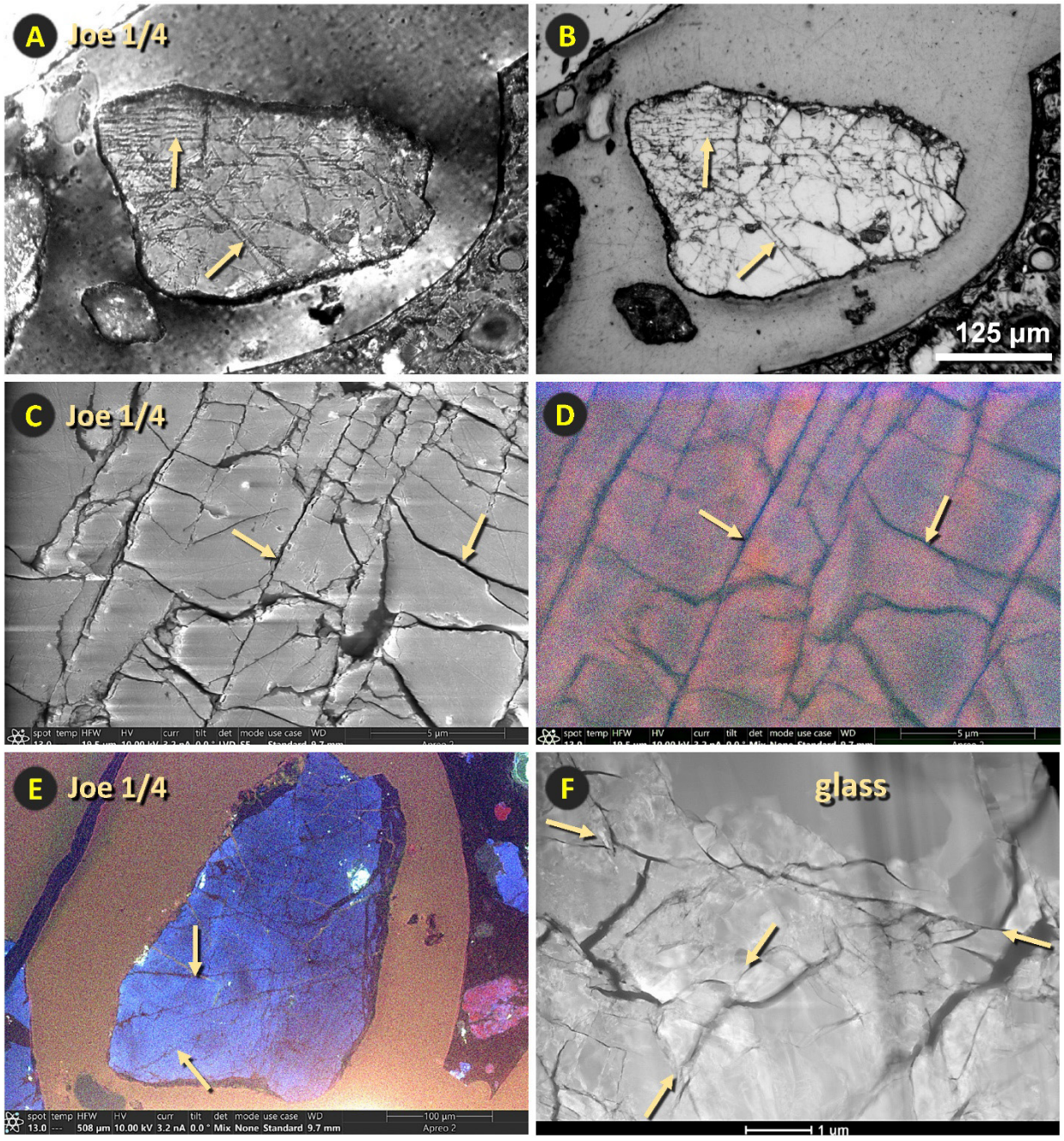

Figure S20. Images of selected portions of shock-fractured quartz grain 12x12 from the Joe-1/4 atomic test site. A) Optical photomicrograph with arrows pointing to selected shock fractures. **(B)** EPI photomicrograph of the same view as panel A. **(C)** SEM image. (**D**) Cathodoluminescence (CL) image shows non-luminescent black lines at arrows indicative of amorphous silica, as confirmed by TEM in panel F. Approximately the same view as in panel C. **(E)** Cathodoluminescence (CL) image shows blue-colored, unshocked quartz matrix containing non-luminescent black lines at arrows indicative of amorphous silica along shock fractures. **(F)** TEM image of oriented and unoriented shock fractures. The notation "glass" marks a darker gray subrounded area composed of amorphous silica.

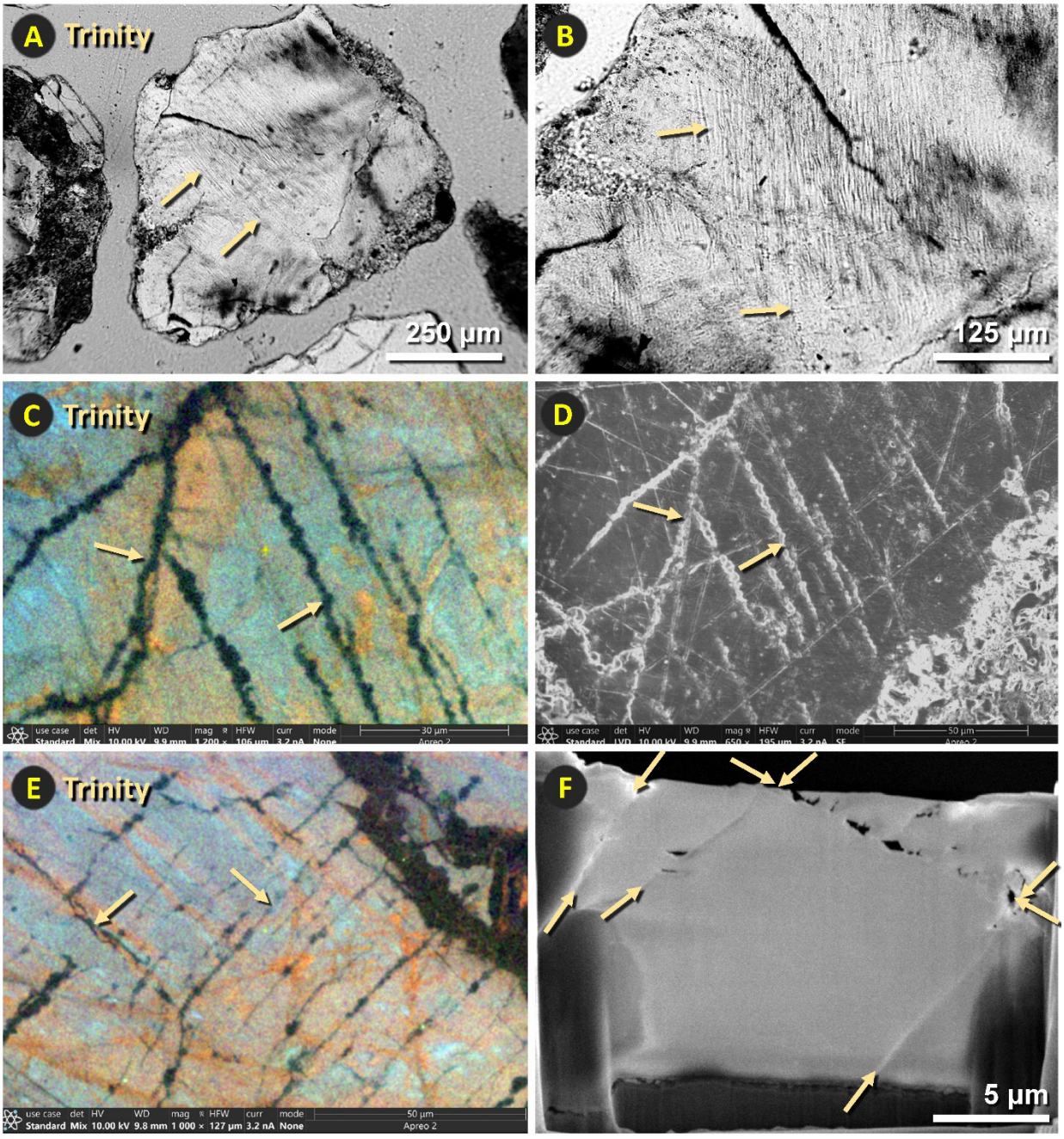

Figure S21. Images of selected portions of shock-fractured quartz grain 30x08 from Trinity JIE grains sample. A) Optical photomicrograph of selected shock fractures at arrows. **(B)** Close-up optical photomicrograph. **(C)** Cathodoluminescence (CL) image of non-luminescent, black lines at arrows indicative of amorphous silica associated with shock fractures, as confirmed by TEM. (**D**) SEM image of approximately the same region of grain as shown in panel C. **(E)** Another CL image of non-luminescent, black lines indicative of the presence of amorphous silica. **(F)** TEM image with arrows marking three directions of shock fractures.

REFERENCES

1. Stöffler, D.; Langenhorst, F. Shock metamorphism of quartz in nature and experiment: I. Basic observation and theory. *Meteoritics* **1994**, *29*, 155-181.
2. Bunch, T.E.; LeCompte, M.A.; Adedeji, A.V.; Wittke, J.H.; Burleigh, T.D.; Hermes, R.E.; Mooney, C.; Batchelor, D.; Wolbach, W.S.; Kathan, J.; et al. A Tunguska sized airburst destroyed Tall el-Hammam a Middle Bronze Age city in the Jordan Valley near the Dead Sea. *Sci Rep* **2021**, *11*, 1-64.
3. Gratz, A. Deformation in laboratory-shocked quartz. *Journal of non-crystalline solids* **1984**, *67*, 543-558.
4. Gratz, A.J.; Fisler, D.K.; Bohor, B.F. Distinguishing shocked from tectonically deformed quartz by the use of the SEM and chemical etching. *Earth and Planetary Science Letters* **1996**, *142*, 513-521.
5. Blenkinsop, T. Shock-induced microstructures and shock metamorphism. *Deformation Microstructures and Mechanisms in Minerals and Rocks* **2000**, 80-89.
6. Bohor, B.; Betterton, W.; Krogh, T. Impact-shocked zircons: discovery of shock-induced textures reflecting increasing degrees of shock metamorphism. *Earth and Planetary Science Letters* **1993**, *119*, 419-424.
7. Bohor, B.; Fisler, D.; Gratz, A.J. Distinguishing between shock and tectonic lamellae with the SEM. In Proceedings of the Lunar and Planetary Science Conference, 1995; p. 145.
8. Hamers, M.; Drury, M. Scanning electron microscope-cathodoluminescence (SEM-CL) imaging of planar deformation features and tectonic deformation lamellae in quartz. *Meteoritics & Planetary Science* **2011**, *46*, 1814-1831.
9. Hamers, M.; Pennock, G.; Drury, M. Scanning electron microscope cathodoluminescence imaging of subgrain boundaries, twins and planar deformation features in quartz. *Physics and Chemistry of Minerals* **2017**, *44*, 263-275.
10. Hamers, M.F. *Identifying shock microstructures in quartz from terrestrial impacts: new scanning electron microscopy methods*; UU Department of Earth Sciences: 2013.
11. Hamers, M.F.; Pennock, G.M.; Herwegh, M.; Drury, M.R. Distinction between amorphous and healed planar deformation features in shocked quartz using composite color scanning electron microscope cathodoluminescence (SEM-CL) imaging. *Meteoritics & Planetary Science* **2016**, *51*, 1914-1931.